PSFC/JA-04-34

Second Harmonic Operation at 460 GHz and Broadband Continuous Frequency Tuning of a Gyrotron Oscillator

M.K. Hornstein, V.S. Bajaj[1], R.G. Griffin[1], K.E. Kreischer[2], I. Mastovsky, M.A. Shapiro, J.R. Sirigiri, and R.J. Temkin

December 2004

Plasma Science and Fusion Center
Massachusetts Institute of Technology
Cambridge, MA 02139 USA

[1]Francis Bitter Magnet Laboratory
Massachusetts Institute of Technology
Cambridge, MA 02139 USA

[2]Northrop Grumman Corporation
Rolling Meadows, IL 60008 USA

Submitted to IEEE Transactions on Electron Devices.

Second Harmonic Operation at 460 GHz and Broadband Continuous Frequency Tuning of a Gyrotron Oscillator

Melissa K. Hornstein, *Student Member, IEEE,* Vikram S. Bajaj, Robert G. Griffin, Kenneth E. Kreischer, *Member, IEEE,* Ivan Mastovsky, Michael A. Shapiro, *Member, IEEE,* Jagadishwar R. Sirigiri, *Member, IEEE,* and Richard J. Temkin, *Fellow, IEEE*

***Abstract*— We report the short pulse operation of a 460 GHz gyrotron oscillator both at the fundamental (near 230 GHz) and second harmonic (near 460 GHz) of electron cyclotron resonance. During operation in a microsecond pulse length regime with 13 kV beam voltage and 110 mA beam current, the instrument generates several watts of power in two second harmonic modes, the $TE_{2,6,1}$ at 456.15 GHz and the $TE_{0,6,1}$ at 458.56 GHz. Operation in the fundamental modes, including the $TE_{0,3,1}$ mode at 237.91 GHz and the $TE_{2,3,1}$ at 233.15 GHz, is observed at output powers up to 70 W. Further, we demonstrate broadband continuous frequency tuning of the fundamental modes of the oscillator over a range of more than 2 GHz through variation of the magnetic field alone. We interpret these results in terms of smooth transitions between higher order axial modes of the resonator. The 460 GHz gyrotron is currently being processed for continuous duty operation, where it will serve as a microwave source for sensitivity-enhanced nuclear magnetic resonance (dynamic nuclear polarization) studies at 16 T (700 MHz ^{1}H), a field strength which is two-fold higher than has been accessible with previous technology.**

***Index Terms*— Gyrotron, submillimeter, harmonic, frequency tuning, dynamic nuclear polarization, nuclear magnetic resonance.**

I. Introduction

THE terahertz or submillimeter band of the electromagnetic spectrum, corresponding to frequencies between 300 and 3,000 GHz, is of considerable interest for applications in spectroscopy, communications, high-resolution RADAR, and imaging [1], [2]. Potential applications are nevertheless frustrated by a historical dearth of sources that yield appreciable powers in this frequency regime. On the one hand, near-infrared lasers are capable of delivering moderate peak power at very high frequencies, but they do not yet scale to intermediate frequencies; on the other hand, conventional vacuum electron devices such as the klystron and traveling wave tube (TWT) operate at very high output powers in the tens of gigahertz, but the physical dimensions of their interaction structures (*i.e.* the region of interaction with the electron beam) necessarily scale with the wavelength. The resulting increase in power density with increasing frequency limits the reliability and utility of these devices above 140 GHz.

Gyrotrons, by contrast, do not suffer from these limitations. Unlike so-called "slow-wave" microwave devices, "fast-wave" devices such as gyrotron oscillators and amplifiers rely on a resonance between the modes of an interaction structure (such as the transverse electric modes of a cylindrical cavity) and the electron beam in a magnetic field. The resonator can be overmoded and, as such, can have physical dimensions which are much larger than the operating wavelength. This permits high peak and average power operation even at elevated frequencies without risk of damage to the interaction structure [3]. Indeed, gyrotrons routinely achieve megawatt power levels at frequencies between 100 and 170 GHz, where plasma heating for fusion is the driving application [4]. The highest frequency achieved by a gyrotron oscillator to date is 889 GHz at Fukui University in Japan [5]. At the University of Electronic Science and Technology of China in Chengdu, a gyrotron successfully produced the third harmonic at 35 GHz [6]. Second harmonic operation of a Soviet gyrotron was demonstrated at 326 GHz with the power level of 1.5 kW at continuous duty [7]. More recent applications in spectroscopy, such as high field dynamic nuclear polarization (DNP) [8] and electron paramagnetic resonance (EPR) require lower peak power, but high average power continuous duty (7-10 days CW) operation and high stability of the frequency and output power.

Superconducting magnet technology is one limiting factor in high frequency gyrotron design. At fields up to 10 T, magnets which have wide room temperature bores generally employ the NbTi superconducting technology; from 10 T to 22 T (corresponding to a range of fundamental electron cyclotron frequency from 280 to 616 GHz), it is necessary to use the Nb_3Sn conductor which elevates the cost of the superconducting magnet. This limitation can be alleviated by operating the gyrotron at a harmonic of electron cyclotron

Manuscript received August 1, 2004; revised November 8, 2004. This work was supported by the NIH under grants no. EB002061, EB002804 and EB002026.

M. K. Hornstein is with the Department of Electrical Engineering and Computer Science and the Plasma Science and Fusion Center, Massachusetts Institute of Technology, Cambridge, MA 02139 USA.

V. S. Bajaj and R. G. Griffin are with the Department of Chemistry and Francis Bitter Magnet Laboratory, Massachusetts Institute of Technology, Cambridge, MA 02139 USA.

K. E. Kreischer is with the Northrop Grumman Corporation, Rolling Meadows, IL 60008 USA.

I. Mastovsky, M. A. Shapiro, and J. R. Sirigiri are with the Plasma Science and Fusion Center, Massachusetts Institute of Technology, Cambridge, MA 02139 USA.

R. J. Temkin is with the Department of Physics and the Plasma Science and Fusion Center, Massachusetts Institute of Technology, Cambridge, MA 02139 USA.

TABLE I
GYROTRON DESIGN PARAMETERS

Frequency	460 GHz	Perp. velocity spread	4%
Magnetic field	8.4 T	Velocity pitch factor	2
Harmonic number	2	Magnetic compression	28
Mode	$TE_{0,6,1}$	Electron beam radius	1 mm
Accelerating voltage	12 kV	Cavity diffractive Q	31,100
Beam current	100 mA	Cavity ohmic Q	19,400
Cathode radius	5.4 mm	Total cavity Q	12,000

resonance, for which the n^{th} harmonic will deliver n times the fundamental frequency for a given magnetic field. However, the harmonic interaction is inherently less efficient than the fundamental interaction due to elevated ohmic losses. It also suffers from the additional complication of mode competition and requires much higher beam currents in order to initiate oscillation. To a large extent, these difficulties can be reduced through appropriate design.

In this work, we report microsecond pulsed results from a 460 GHz gyrotron oscillator designed to operate continuously at the second electron cyclotron harmonic at low voltages and output powers of between several watts and several tens of watts. Further, we have demonstrated that continuous tuning of the gyrotron oscillator over a range of nearly 2 GHz at constant output power is possible by changing the magnetic field and implementing feedback control on the beam current. The gyrotron oscillator design will also permit the precise control of the output power and frequency that is necessary for applications to sensitivity-enhanced magnetic resonance spectroscopy through dynamic nuclear polarization (DNP). Originally employed to produce spin polarized targets for nuclear scattering experiments, DNP is a technique through which the greater Zeeman polarization of the electrons is transferred to the nuclei, in this case to enhance the sensitivity of a subsequent NMR experiment by up to two orders of magnitude. DNP requires irradiation of the sample with 1–10 W of power near the electron Larmor frequency (which is close to the electron cyclotron frequency) [8]. This technology will extend the applicability of DNP techniques to frequencies much higher than was previously possible.

II. GYROTRON DESIGN CONSIDERATIONS AND CONSTRUCTION

The design of the 460 GHz gyrotron oscillator is based on a previous 250 GHz oscillator built at MIT for DNP experiments [9]–[11], with the additional goal that it operate at the second electron cyclotron harmonic. This design is described in [12], [13]. Challenges associated with second harmonic operation were addressed with novel designs for many components of the tube. Critical operational features of this design include the ability to efficiently generate second harmonic radiation at relatively low voltages and currents, low starting currents, reduced ohmic losses for higher efficiency, and isolated excitation of a second harmonic mode without competition from fundamental modes.

A schematic of the 460 GHz gyrotron system is shown in Fig. 1. The axis of the gyrotron tube and electron beam

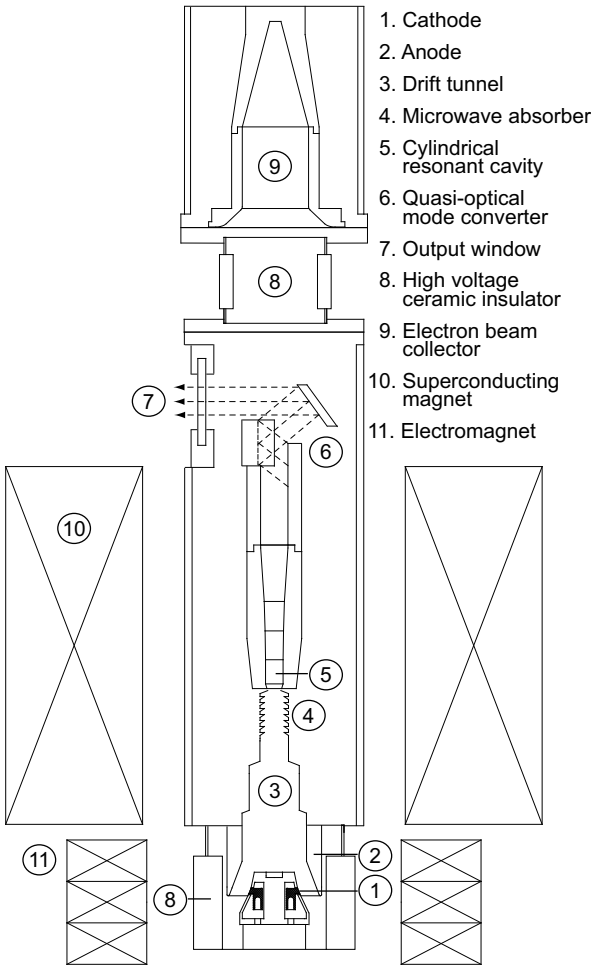

Fig. 1. Cross-sectional schematic of the cylindrically symmetric 460 GHz gyrotron tube, not shown to scale, indicating key components. The gyrotron tube is approximately 1.4 m long and the magnet bore diameter is 7.62 cm

lie along the vertical bore of a 9.2 T superconducting magnet, while the microwave power is extracted via a quasi-optical mode converter through an auxiliary, horizontal, room temperature bore which intersects with the main bore above the main coil of the superconducting magnet. The dual-bore arrangement allows for efficient separation of the microwave beam from the electron beam, resulting in increased vacuum pumping conductance to the lower portion of the tube, a feature which is critical for continuous duty operation. It also reduces ohmic losses in the output waveguide, simplifies the window design, and allows the spent electron beam to be collected in a highly compact and water-cooled collector region which is far from any fragile microwave or waveguide structure. The total length of the gyrotron tube is therefore only 1.4 m. Sets of two-axis horizontal alignment stages are located both under the electron gun and around the collector and are used to align the gyrotron tube with respect to the magnetic field of the superconducting magnet thereby aligning the electron beam.

The experiment employs a low voltage, diode-type electron gun whose design is modeled after the gun employed in a successful 250 GHz gyrotron experiment [11]. The low operating voltage of less than 15 kV eliminates the need

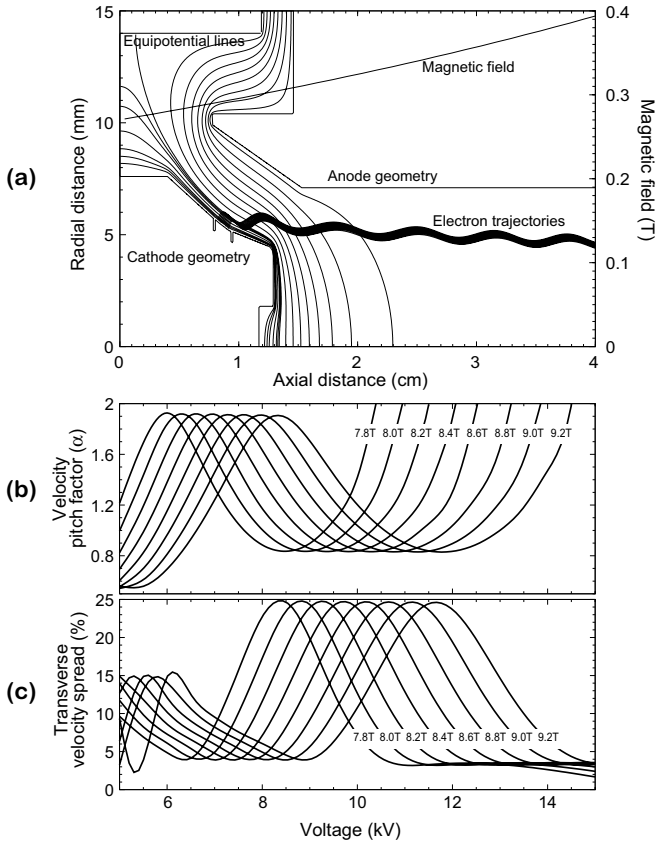

Fig. 2. Simulation of the evolution of the transverse and axial velocities of the electrons accelerated at 12 kV in the 460 GHz gyrotron experiment using the EGUN electron optics and gun design program. (a) The electron trajectories, equipotential lines, cathode and anode geometries, and applied magnetic field of the gun region. (b) Velocity pitch factor and (c) transverse velocity spread for the low-voltage, diode-type gun used in the 460 GHz gyrotron experiment. Each curve is derived from EGUN simulations of the gun geometry conducted as a function of voltage and magnetic field.

for cumbersome oil cooling and high voltage insulation and reduces the possibility that ionizing radiation will be produced. The reduced complexity of this gun design is achieved at the expense of an increased sensitivity of the electron beam velocity pitch factor and velocity spread to the exact operating parameters. For that reason, characteristics of the electron gun were studied using the EGUN electron optics and gun design program [14] and optimized for the intended operating regime. Figure 2(a) depicts a typical simulation of the trajectories followed by electrons accelerated by a 12 kV potential in a gently tapered magnetic field reaching a maximum of 8.4 T in the cavity. The transverse rms velocity spread and beam α reach 4% and 2, respectively, in the region of the cavity for the design parameters optimized for second harmonic operation. For operating parameters corresponding to excitation of fundamental modes observed in this experiment, EGUN simulations predict large variations in the velocity spread and velocity pitch ratio with changes in the beam voltage and the magnetic field. The results of an EGUN study of this gun over a broader range of operating voltages and magnetic fields are shown in Figure 2(b) and (c).

In practice, the electron beam parameters such as the velocity pitch factor and velocity spread can be experimentally

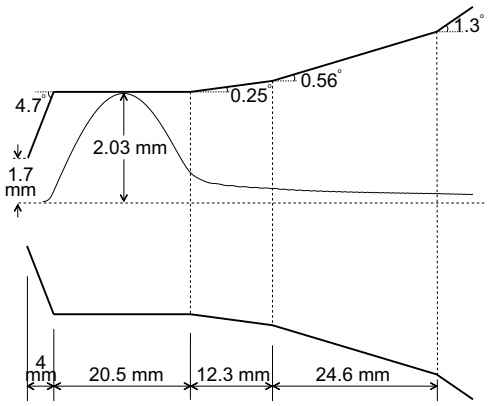

Fig. 3. Cross-sectional schematic, not drawn to scale, of the 460 GHz gyrotron cavity with the axial radiation field profile for the second harmonic $\mathrm{TE}_{0,6,1}$ resonator mode.

tuned by an electromagnet shim coil situated around the electron gun through changing the magnetic compression, the ratio of axial magnetic field at the cavity and cathode. Also known as the "gun coil", it reaches a maximum magnetic field of 8.5×10^{-2} T on axis and serves to fine tune the electron beam characteristics.

The resonant gyrotron interaction structure is a tapered cavity that was optimized for the $\mathrm{TE}_{0,6,1}$ second harmonic eigenmode at 460 GHz using a cold cavity (electron beam absent) simulation code described in Section IV-B [15]. Figure 3 is a cross-sectional schematic of the tapered cavity, consisting of a straight section of length 20.5 mm and circular cross-section of radius 2.03 mm joined to a linearly uptapered section at three discrete slopes at the exit (0.25, 0.56, and 1.3^o) and a linearly downtapered section at the entrance of 4.7^o, showing the axial profile of the design mode. Mode conversion in the input taper was not detected by simulation. The gyrotron cavity was electroformed from OFC copper using an aluminum mandrel precision machined to a 5 μm tolerance and 0.2 μm finish.

The quasi-optical mode converter, optimized for the $\mathrm{TE}_{0,6}$ mode, serves to convert the waveguide radiation into a free-space Gaussian beam in addition to separating the electron beam from the RF beam. The mode converter consists of a step cut waveguide launcher, a focusing mirror, and a flat reflecting mirror.

Table I summarizes the gyrotron and cavity design parameters. Notably, the gyrotron was designed for low voltage and current (12 kV, 100 mA) operation in a single second harmonic higher order mode. The DNP experiment requires moderate peak powers but continuous duty cycle operation for periods lasting 7-10 days, during which the output power and frequency must be stable to within 1% and at least 5 MHz respectively. We selected the $\mathrm{TE}_{0,6,1}$ design mode on the basis of its isolation from competing fundamental modes and because the electron gun can easily generate a 1 mm beam radius in the cavity, which couples to the third maximum of the transverse field distribution.

Auxiliary equipment includes a recirculating chiller with three separate channels to water cool the electron beam col-

lector, gun coil, and to maintain a constant cavity temperature, which is required for gyrotron frequency stability.

A. Theory

The electromagnetic radiation in a gyrotron is produced by the interaction of a mildly relativistic gyrating electron beam and transverse electric (TE) wave near cutoff in an overmoded cavity resonator situated in a DC magnetic field. The oscillation frequency ω of a $\mathrm{TE}_{m,p,q}$ mode of a cylindrical cavity of effective length L and radius r_0 is given by

$$\frac{\omega^2}{c^2} = k^2 = k_\perp^2 + k_z^2, \tag{1}$$

where $k_\perp$ $(= \nu_{mp}/r_0)$ and k_z $(= q\pi/L \ll k_\perp)$ are the transverse and longitudinal propagation constants of the $\mathrm{TE}_{m,p,q}$ wave, c is the velocity of light, ν_{mp} is the p^{th} root of $J'_m(x)$, and m, p, and q are, respectively, the azimuthal, radial, and axial mode numbers. The resonance condition for the excitation of the cyclotron resonance maser instability is satisfied when ω and k_z in (1) satisfy the beam mode dispersion relation,

$$\omega - k_z \beta_{z0} c \approx n\omega_{c0}, \tag{2}$$

where ω_{c0} $(= eB_0/\gamma m_e)$ is the relativistic cyclotron frequency, $\gamma = (1 - \beta_{z0}^2 - \beta_{\perp 0}^2)^{-1/2}$ is the relativistic mass factor, m_e and e are the electron rest mass and charge, $\beta_{\perp 0}$ and β_{z0} are, respectively, the transverse and longitudinal velocities of the electrons normalized to the velocity of light, n is the cyclotron harmonic number, B_0 is the magnitude of the static axial magnetic field, and the subscript "0" denotes that the value is taken at the start of the interaction region.

The starting current is defined as the minimum electron beam current needed to overcome the dissipative processes in the cavity and excite a given transverse electric mode. This threshold is obtained on energy conservation grounds by equating the dissipative relationship implied in

$$P = \frac{\omega W}{Q} \tag{3}$$

with the beam-wave power transfer governed by

$$P = -\frac{1}{2}\mathrm{Re}\left\{\int \mathbf{E}^* \cdot \mathbf{J}\ d\mathbf{r}\ d\mathbf{p}\right\}, \tag{4}$$

where W is the stored energy of the mode, $\mathbf{E}$ is the cavity electric field, $\mathbf{J}$ $(= e\mathbf{v}f(\mathbf{r},\mathbf{p},t))$ is the current density, and $f(\mathbf{r},\mathbf{p},t)$ is the electron distribution function. For both the fundamental and second electron cyclotron harmonic, the starting current, in amperes, for a Gaussian axial field profile with a single axial maximum, as a function of the magnetic field detuning is given by [16]:

$$I_{\mathrm{start}}(\Delta,\mu) = 8.56\times 10^4 \frac{\exp\left[\frac{1}{8}(\mu\Delta)^2\right]}{\mu^2(\mu^2\Delta - 4n)}\left(\frac{\gamma_0}{Q_T}\right)\beta_{\perp 0}^{2(3-n)} \times \left(\frac{L}{\lambda}\right) C_{m,p}^{-2}, \tag{5}$$

where the length parameter μ is defined by

$$\mu \equiv \pi \frac{\beta_{\perp 0}^2}{\beta_{\parallel 0}} \frac{L}{\lambda}, \tag{6}$$

the magnetic field detuning Δ is given by

$$\Delta = \frac{2}{\beta_{\perp 0}^2}\left(1 - n\frac{\omega_{c0}}{\omega}\right), \tag{7}$$

the beam-wave coupling factor $C_{m,p}^2$ is given by

$$C_{m,p}^2 = \frac{J_{m\pm n}^2(k_\perp R_e)}{\left(\nu_{mp}^2 - m^2\right) J_m^2(\nu_{mp})}, \tag{8}$$

and R_e is the electron beam radius. The "$\pm$" sign in (8) refers to the counter- and co-rotating $\mathrm{TE}_{m,p}$ waves, respectively.

A similar theory, derived for the case of fixed sinusoidal axial field profiles, can be applied to calculate linear starting currents for higher order axial modes [17].

B. Operation at the second harmonic

Operation of a gyrotron at the second harmonic of the electron cyclotron resonance, which results in approximately twice the fundamental frequency for a given magnetic field, is attractive even when magnet technology is not a limiting factor. Nevertheless, it suffers from three principal challenges: high ohmic losses, which reduce the efficiency, high start currents, which require higher beam power than our experimental design allows, and finally, mode competition. Of these, mode competition from fundamental modes whose starting currents are inherently lower is the primary concern. Due to the density of the mode structure in an overmoded resonator, particularly when higher order longitudinal modes are included, mode competition must be explicitly addressed in the design [18].

The ratio of the second electron cyclotron harmonic, $I_{2\omega_c}$, to the fundamental starting current, I_{ω_c}, can be approximated from (5) as follows;

$$\frac{I_{2\omega_c}}{I_{\omega_c}} = \frac{(L/\lambda)_{\omega_c}^2}{(L/\lambda)_{2\omega_c}^2} \times \frac{1}{\beta_{\perp 0}^2} \times \frac{Q_{\omega_c}}{Q_{2\omega_c}} \times \frac{(C_{m,p})_{\omega_c}^2}{(C_{m,p})_{2\omega_c}^2}, \tag{9}$$

where the subscript ω_c denotes the fundamental mode quantities and $2\omega_c$ the second harmonic. The first term is approximately $\frac{1}{4}$ since the number of wavelengths in a cavity of fixed length L is approximately twice as large at second harmonic as at the fundamental. Due to the low voltage used to accelerate the electrons, the second term, which incorporates the normalized transverse velocity of the electrons, is large; it is about 25 for velocity pitch factor equal to 2 at 12 kV. In practice, this can be mitigated through a design in which the second harmonic Q is large with respect to the competing fundamental mode. In this experiment, the value of the third factor is about $\frac{1}{3}$. The fourth factor is the ratio of beam-wave coupling factor $C_{m,p}^2$ of the modes and depends on the beam radius. It is generally greater than unity because the ν_{mp}^2 term is smaller at the fundamental than at the second harmonic. In summary, the minimum starting current for the second harmonic modes is generally at least several times higher than the minimum starting current for the fundamental modes.

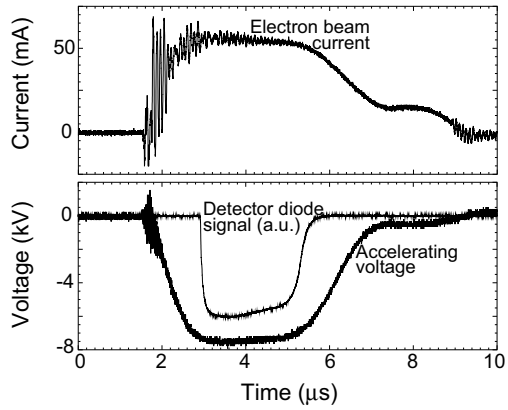

Fig. 4. Oscilloscope microwave signal, beam voltage and collector current traces of the fundamental $TE_{0,3,1}$ mode at 237.91 GHz and main magnetic field of 8.58 T. The RF signal is recorded with a broadband WR-3 (220-325 GHz) detector diode. The voltage and current traces are measured through inductively couples probes (Rogowsky coils).

In lowering the start current through lengthening the cavity, we encounter an elevated diffractive Q,

$$Q_{\text{diffractive}} \propto \left(\frac{L}{\lambda}\right)^2, \tag{10}$$

which directly leads to increased ohmic losses in the cavity by

$$\eta \propto \frac{Q_{\text{ohmic}}}{Q_{\text{diffractive}} + Q_{\text{ohmic}}}, \tag{11}$$

where η is the total efficiency. In reality, the cavity design must be a compromise between several factors.

III. Second Harmonic Experiment

The initial experiments were performed using pulses with duration of approximately 3 μs. The free parameters of the experiment include the electron beam voltage and current, main magnetic field, gun magnetic field, and the alignment of the vacuum tube with respect to the room temperature bore of the superconducting gyrotron magnet. The electron beam voltage and current were varied up to 15 kV and 160 mA while the main magnetic field was varied up to 9.2 T and the gun magnet up to $\pm 8.5 \times 10^{-2}$ T with respect to the cathode field. All measurements were taken at the end of a 2 m long copper waveguide of 2.54 cm inner diameter, which couples to the output window.

Figure 4 shows an example of typical oscilloscope traces of the electron beam voltage, collector current, and RF signal for the experiment. In this case we show the fundamental $TE_{0,3,1}$ mode. The noise and distortions to the pulse shape are due to power supply ripple and the transient response of connecting cables. A small droop in the voltage pulse causes a small corresponding droop in the microwave pulse.

A. Start oscillation current

The starting current curves for all modes experimentally observed are shown in Fig. 5. Five fundamental modes are depicted with open shapes ranging in frequency from 157 to 246 GHz and two second harmonic modes near 460 GHz are shown with filled shapes. Data in each mode were collected at the unique voltage which was optimal for its excitation. The conditions are labeled in Fig. 5.

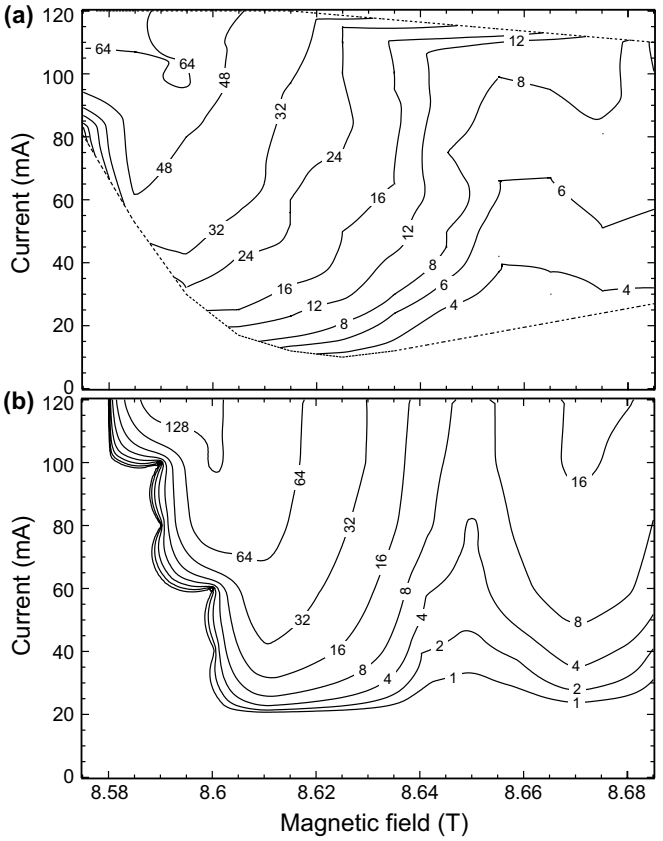

Fig. 6. Contour plot of (a) measured peak power data of the fundamental $TE_{0,3,q}$ modes in watts as a function of beam current and magnetic field using a pyroelectric detector. The electron gun was pulsed for several microseconds at a repetition rate of approximately 30 Hz with 9 kV. The power level was calibrated using a calorimeter. (b) MAGY simulated power at experimental conditions.

B. Power

Peak power measurements were made during the microsecond pulsed experiment using both a laser calorimeter and a pyroelectric detector. The calorimeter head surface was coated with an absorbing layer of paint and re-calibrated for millimeter wavelengths.

Figure 6(a) depicts measured peak power data of the fundamental $TE_{0,3,q}$ modes around 238 GHz as a function of beam current and magnetic field. A pyroelectric detector was used to measure the radiation, and the beam voltage was fixed at 9 kV with microsecond pulse lengths and a repetition rate of approximately 30 Hz. The data were confirmed with calorimetric measurements. Nearly 70 W of peak power were recorded at 237.9 GHz with an efficiency of over 7%.

Initial pulsed power measurements of the $TE_{2,6,1}$ (456.15 GHz) second harmonic mode indicate signal strengths of several watts with 13 kV and 110 mA. The $TE_{2,6,1}$ mode was found experimentally to be more isolated from fundamental modes than the $TE_{0,6,1}$ second harmonic design mode, which was also observed in [19], [20].

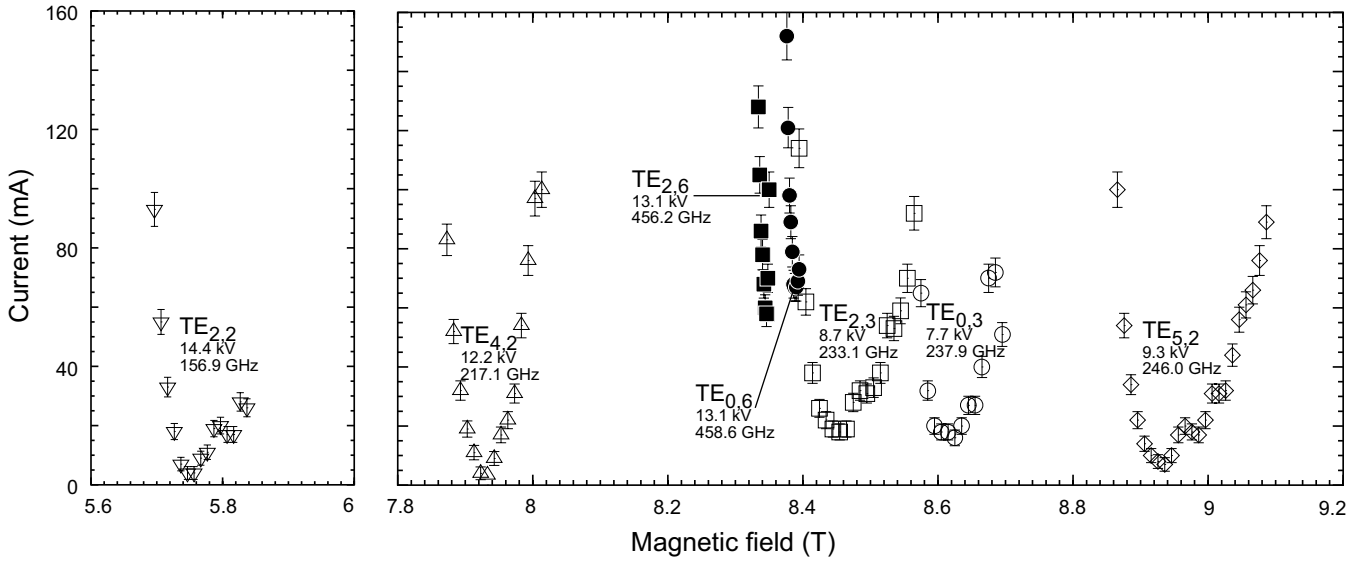

Fig. 5. Summary of experimental starting current data recorded for resonant cavity modes from 5.6 to 9.2 T and up to 15 kV and 160 mA. Open symbols denote fundamental modes and filled-in symbols denote second harmonic modes.

TABLE II

MINIMUM START CURRENT, AND MAGNETIC FIELD AND FREQUENCY FOR MINIMUM STARTING CURRENT OF $q = 1$ MODES FROM LINEAR THEORY [21] USING EGUN CALCULATED PARAMETERS OF FIG. 2(B) AND (C) VS. EXPERIMENT

$\mathbf{TE}_{m,p,q}$	Experiment			Theory		
	B_0 (T)	I_{st} (mA)	f (GHz)	B_0 (T)	I_{st} (mA)	f (GHz)
$TE_{2,2,1}$	5.747	4	156.90	5.746	4	156.89
$TE_{4,2,1}$	7.933	2	217.10	7.926	4	217.09
$TE_{2,6,1}$	8.346	58	456.15	8.345	58	456.15
$TE_{0,6,1}$	8.388	67	458.56	8.390	67	458.56
$TE_{2,3,1}$	8.454	18	233.15	8.433	27	233.15
$TE_{0,3,1}$	8.625	16	237.91	8.605	7	237.92
$TE_{5,2,1}$	8.936	7	246.00	8.915	14	246.01

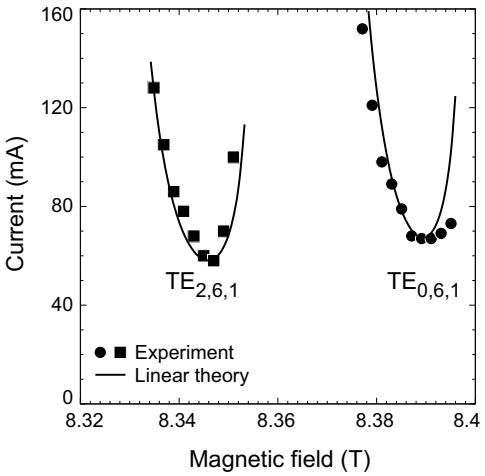

Fig. 7. Second harmonic $TE_{2,6,1}$ and $TE_{0,6,1}$ start oscillation current data (points) compared with linear theory (solid lines) at 13.1 kV.

C. Linear theory and MAGY simulations

With the linear theory previously described in Section II-A, we can proceed to analyze the start current data from Fig. 5. In all cases, we use the beam parameters that were derived from EGUN simulations. We have observed two second harmonic modes in these experiments, the $TE_{2,6,1}$ and $TE_{0,6,1}$, for which theoretically predicted and experimentally measured starting currents show good agreement (Figure 7). For each mode, we have also calculated the theoretical magnetic field which minimizes the start current and compared it to experiment (Table II). Finally, we are able to calculate a cavity radius of 2.041 mm to obtain the best fit to the data. This value is 0.3% larger than the design value of 2.035 mm and the difference is within the manufacturing accuracy of the cavity.

It is clear that the $TE_{m,p,1}$ modes are excited at the magnetic fields predicted by linear theory [21]. However, the fundamental modes in the experiment have multiple local minima which form a continuous manifold of accessible cavity oscillation states, each one producing monochromatic emission. This phenomenon, which is due to higher order longitudinal states, will be more fully discussed in Section IV. In short, for fundamental modes, the occurrence of overlapping $TE_{m,p,q}$ (where q is larger than one) higher order axial modes broadens the magnetic excitation range. Finally, the very low values of start current observed in the fundamental modes are described by linear theory.

In Table II, the experimental start current values of seven observed modes are compared with values calculated from [21] using beam parameters from Fig. 2, diffractive Q from cold cavity theory, and all other values from experiment. The agreement is good, and discrepancies might be explained by the uncertainties in the beam alpha, diffractive Q, and experimental conditions such as beam radius and alignment.

Nonlinear modeling has been performed using the time-dependent simulation code MAGY, developed jointly at the University of Maryland and the Naval Research Laboratory

[22]. In MAGY, the resonator transverse fields are expanded in a normal mode basis of waveguide modes, and the axial field structure is solved self-consistently in the slowly time-varying approximation. In all the simulations presented here, one or two TE modes were used in the basis. In order to observe steady state dynamics, all modes were forced to oscillate at the frequencies obtained from self-consistent simulations in an iterative adjustment procedure which employs the slope of the field phase evolution as an estimator. The cavity geometry was defined with an axial grid step of of 9.8×10^{-3} cm (1041 points), and with half the conductivity of ideal copper. We have chosen physical parameters to describe the geometry and thermal properties of the beam. This includes, for all simulations, pitch angle, velocity spread, guiding center radius and (where applicable) the spread in guiding centers which was obtained from EGUN simulations presented in Figure 2(b) and (c). We have systematically increased the EGUN-derived velocity spread according to [23] to account for cathode uniformity, thermal variations, and other effects not explicitly modeled in EGUN. The simulation geometry also involves a slightly tapered magnetic field derived from experimental measurement of the axial field profile. The simulation time step was taken to be 50-150 ps, and we ran the code for 200-2,000 iterations to reach a converged steady state solution.

In simulations of the $\mathrm{TE}_{0,3}$ fundamental mode, MAGY qualitatively reproduces the experimentally observed power distribution (Figure 6(b)) but predicts much higher power output than was actually observed. The remaining differences might arise due to higher ohmic losses in the cavity, diffractive and coupling losses in the quasi-optical mode converter, and reduced coupling to the output waveguide, which were not studied in detail in this experiment.

IV. Broadband continuous frequency tuning experiment

Broadband continuous frequency tuning was observed as a function of magnetic field for all fundamental modes. A long cavity design was utilized in order to reduce the start current for the second harmonic, in order to meet excitation criteria for a low power gun. In addition to lowering the start current for second harmonic modes, the length of the cavity permits multiple radiation maxima along the axial length of the cylindrical waveguide resonator to be excited. That is, in addition to the $\mathrm{TE}_{m,p,1}$ modes that we expect to excite, there exist a series of $\mathrm{TE}_{m,p,q}$ modes where the q is larger than one. These higher order axial modes can be excited at magnetic fields just above those where the $\mathrm{TE}_{m,p,1}$ modes are reached. The practical consequence of this is that continuous frequency tuning on the order of several gigahertz has been observed for each of the fundamental modes excited in this gyrotron. A continuous bandwidth of 410 MHz around 31.8 GHz has been previously observed using higher order axial modes, up to $q = 5$, in a two-stage gyrotron amplifer experiment at the University of Maryland [24]. Several experiments in electron paramagnetic resonance (EPR) and dynamic nuclear polarization (DNP) might be dramatically simplified with a tunable oscillator that exploits this property.

A. Experimental data

The experimental gyrotron frequency corresponding to magnetic field tuning in the range 5.6 - 9.2T is shown in Figure 8. The frequency was measured using a heterodyne receiver system which operates on a high harmonic of an 18-26 GHz YIG-tuned local oscillator. The local oscillator was frequency-locked using a PLL circuit, resulting in frequency measurement accuracy which is limited only by the harmonic phase noise of the local oscillator.

The data were taken concurrently with the data from Fig. 5, in which the beam current was set near the threshold of oscillation for each mode. Further, the data in each $\mathrm{TE}_{m,p}$ mode were taken at unique voltages which are labeled on Fig. 5. We observe continuous frequency tuning in each fundamental mode across a range of magnetic fields. The frequency tuning bandwidth is relatively large, notably with 1.8 GHz tuning at the 246 GHz $\mathrm{TE}_{5,2,q}$ modes and 2.34 GHz tuning at the 157 GHz $\mathrm{TE}_{2,2,q}$ modes. Further, the data show that a significant amount of power can be maintained across the frequency tuning range of a given mode. This is illustrated for the $\mathrm{TE}_{0,3,q}$ modes in Fig. 6(a), where the power measurements are taken as a function of the magnetic field and electron beam current. We can conclude that an average power of at least 5 W can be maintained from 237.9 to 238.6 GHz. Finally, the second harmonic modes do not tune by more than 20-30 MHz, which implies that the long-term frequency will be stable towards drift in the magnetic field. This follows from Fig.7 where we have shown that only the first axial variation of the second harmonic modes has been excited in this experiment. This is important in the intended application of this device.

B. Discussion

Prior to further analysis, we note that the mechanism of frequency tuning is qualitatively similar for each fundamental mode. Figure 9 is a plot of the experimental data from the fundamental modes of Figs. 5 and 8, normalized to one magnetic field axis. That is, the data from each $\mathrm{TE}_{m,p,q}$ mode family are normalized to the magnetic field value which yields minimum start current for the mode. The frequency axis in the lower plot is then normalized with respect to the frequency of the first axial mode at that magnetic field.

The start currents and normalized frequency tuning with respect to magnetic field resemble each other in functional form. For instance, in the upper plot, the local minima of the start oscillation current curves fall at approximately the same magnetic field values; in the lower plot, the frequency tuning rate, df/dB, is identical for each family of modes.

For the following discussion, we therefore focus our attention on the $\mathrm{TE}_{5,2}$ mode, which displays broad frequency tuning in isolation from other fundamental and second harmonic modes. First, using weakly irregular waveguide (so-called "cold cavity") theory [15], we can calculate the resonator eigenfrequencies, Q values, and axial field functions of TE modes by solving a one-dimensional wave equation of the form

$$\left[\frac{d^2}{dz^2} + k_z^2(z)\right] f(z) = 0, \tag{12}$$

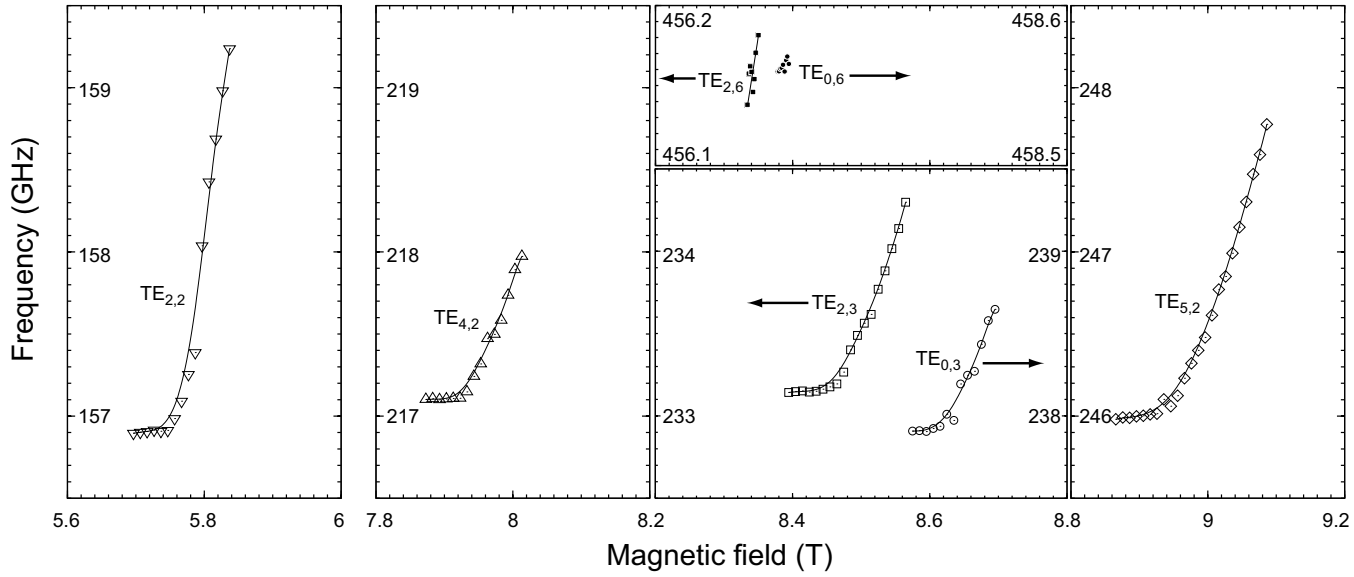

Fig. 8. Summary of experimentally measured frequency vs. magnetic field for the modes in Fig. 5.

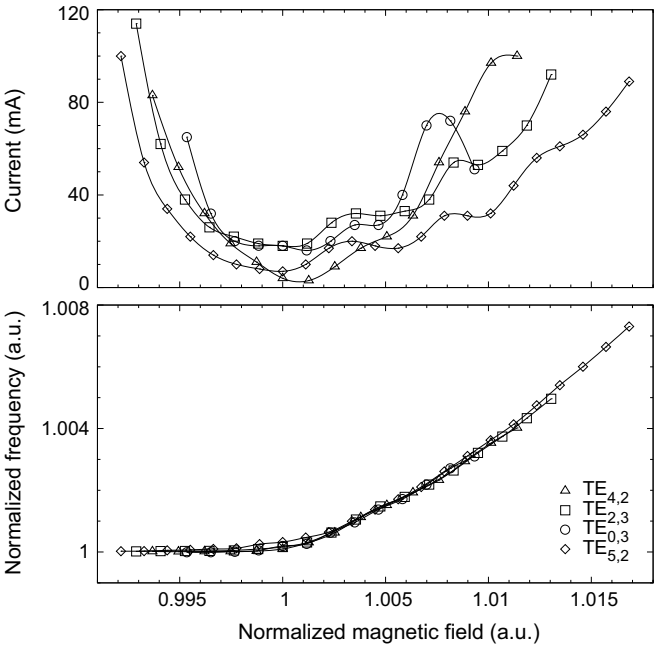

Fig. 9. Start oscillation currents and frequency tuning normalized to the frequency at the minimum start current versus magnetic field normalized to the field at the minimum start current of fundamental modes from 7.8 to 9.2 T.

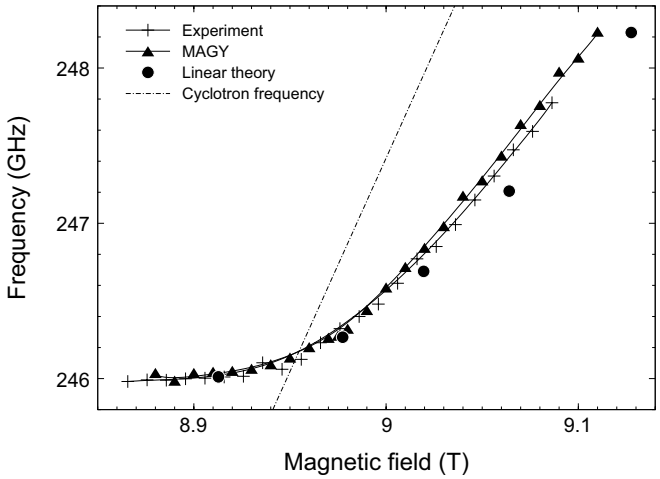

Fig. 10. Linear theory (solid circles) and MAGY simulation (solid triangles) using EGUN calculated parameters of the frequency tuning of the $TE_{5,2,q}$ modes compared to the experiment (+). The dotted line is the relativistic cyclotron frequency.

where f is the longitudinal profile function and z is the longitudinal coordinate, with the boundary conditions of a cutoff wave in the input and propagating wave at the output. The analysis relies upon the dimensions of the cavity as well as the indices of the $TE_{m,p}$ mode, but neglects coupling to other modes and the perturbing effects of the electron beam. Calculated field profiles lose the distinction between consecutive axial modes, approximating the continuous behavior observed in the experiment.

Using the cold cavity frequencies and axial field profiles corresponding to the $TE_{5,2,1}$–$TE_{5,2,5}$ modes, we have applied linear theory [21] to calculate their corresponding magnetic fields. These five calculated eigenfrequencies are shown in Fig. 10 as solid circles, where each eigenfrequency is located at the magnetic field corresponding to the theoretical minimum starting current of that eigenmode. This value of magnetic field is selected because, at the minimum starting current, the effect of dispersion due to the electron beam is negligible and the linear theory should be valid. Since these data are indeed taken near the threshold of the starting current, the agreement between theory and experiment is very good.

However, the linear theory alone cannot completely describe the dynamics of the beam-wave interaction for reasons that have been previously enumerated. For example, the observation of continuous frequency tuning even between frequencies corresponding to the discrete axial modes of the cold cavity theory cannot be easily explained within the framework of

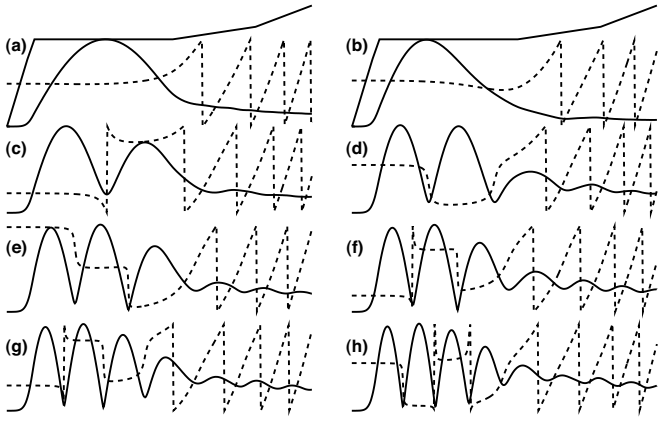

Fig. 11. Self-consistent axial field profiles for $TE_{5,2,q}$ modes with $q \geq 1$ as calculated from MAGY. The cavity geometry is indicated above each column, and we have displayed the normalized voltage amplitude. The frequency increases from 246.0 GHz in (a) to 248.1 GHz in (h).

linear theory. We therefore again apply the non-linear, time-dependent theory as implemented in MAGY to model the operating characteristics of this gyrotron. Using the EGUN-derived beam pitch ratio and the adjusted perpendicular velocity spread to model thermal properties of the electron beam as previously described, the self-consistent MAGY simulations quantitatively predict continuous frequency tuning and monochromatic emission in the $TE_{5,2}$ mode. The agreement between experiment and the predictions of MAGY as shown in Fig. 10 is better than for the linear theory, even though the former depends on fewer adjustable parameters.

Detailed analysis of the axial field structures predicted by MAGY (Figure 11) reveal a continuous transition from lower to higher order axial modes, and this is the basis of the observed frequency tuning. The self-consistent axial field structures resemble those obtained from the cold cavity theory.

V. Conclusion

The 460 GHz experiment has successfully demonstrated that a gyrotron can efficiently produce several watts of average power in submillimeter wavelengths at low voltage. In addition, continuous broadband frequency tuning of the gyro-oscillator has been demonstrated, and we have presented non-linear and linear analyses of the results. The gyrotron is currently being processed for CW second harmonic generation at 460 GHz. We note that, due to the inhomogeneous frequency dispersion of the interactions responsible for dynamic nuclear polarization effects in paramagnetically doped solids, either the microwave source frequency or the static magnetic field in the NMR spectrometer must be varied over a broad range to optimize the experiment. Performing the latter currently requires high homogeneity superconducting magnets in the 9–16 T range which incorporate a persistent sweep coil. Future oscillator designs which could exploit the broad tunability features described here might eliminate this complication of the experiment while still preserving the advantages of simple, low-voltage, CW operation.

Acknowledgment

The authors wish to thank Dr. Alexander Vlasov for helpful discussions. The authors would also like to thank Bill Mulligan, Peter Allen, Ajay Thakkar, and Bob Childs for technical assistance. VSB acknowledges receipt of an NSERC PGS Fellowship. This research was supported by the National Institutes of Health through grants no. EB002061, EB002804 and EB002026.

References

[1] F. C. de Lucia, "Science and technology in the submillimeter region," *Optics and Photonics News*, vol. 14, no. 8, pp. 44–50, Aug. 2003.

[2] D. van der Weide, "Applications and outlook for electronic terahertz technology," *Optics and Photonics News*, vol. 14, no. 4, pp. 48–53, Apr. 2003.

[3] K. Felch, B. Danly, H. Jory, K. Kreischer, W. Lawson, B. Levush, and R. Temkin, "Characteristics and applications of fast-wave gyrodevices," *Proceedings of the IEEE*, vol. 87, no. 5, pp. 752–81, May 1999.

[4] R. Callis, W. Cary, S. Chu, J. Doane, R. Ellis, K. Felch, Y. Gorelov, H. Grunloh, J. Hosea, K. Kajiwara, J. Lohr, T. Luce, J. Peavy, R. Pinsker, D. Ponce, R. Prater, M. Shapiro, R. Temkin, and J. Tooker, "Maturing ECRF technology for plasma control," *Nuclear Fusion*, vol. 43, no. 11, pp. 1501–1504, Nov. 2003.

[5] T. Idehara, I. Ogawa, S. Mitsudo, M. Pereyslavets, N. Nishida, and K. Yoshida, "Development of frequency tunable, medium power gyrotrons (gyrotron FU series) as submillimeter wave radiation sources," *IEEE Trans. on Plasma Sci.*, vol. 27, no. 2, pp. 340–354, Apr. 1999.

[6] H. Li, Z. Xie, W. Wang, Y. Luo, P. Du, X. Den, H. Wang, S. Yu, X. Niu, L. Wang, and S. Liu, "A 35-GHz low-voltage third-harmonic gyrotron with a permanent magnet system," *IEEE Trans. Plasma Sci.*, vol. 31, no. 2, pp. 264–271, Apr. 2003.

[7] N. Zaytsev, T. Pankratova, M. Petelin, and V. Flyagin, "Millimeter- and submillimeter-wave gyrotrons," *Radiophys. Quantum Electron.*, vol. 19, pp. 103–104, 1974.

[8] V. Bajaj, C. Farrar, M. Hornstein, I. Mastovsky, J. Vieregg, J. Bryant, B. Elena, K. Kreischer, R. Temkin, and R. Griffin, "Dynamic nuclear polarization at 9 Tesla using a novel 250 GHz gyrotron microwave source," *J. Mag. Res.*, vol. 160, no. 2, pp. 85–90, Feb. 2002.

[9] K. Kreischer, C. Farrar, R. Griffin, and R. Temkin, "The use of a 250 GHz gyrotron in a DNP/NMR spectrometer," *Proc. 23rd Intl. Conf. Infrared and Millimeter Waves*, pp. 357–341, 1998.

[10] K. E. Kreischer, C. T. Farrar, R. G. Griffin, R. J. Temkin, and J. Vieregg, "The development of a 250 GHz CW gyrotron for EPR and NMR spectroscopy," *Proc. 24th Int. Conf. Infrared and Millimeter Waves*, 1999.

[11] K. E. Kreischer, C. Farrar, R. Griffin, R. Temkin, and J. Vieregg, "A 250 GHz gyrotron for NMR spectroscopy," *Proc. 27th Int. Conf. on Plasma Sci.*, p. 198, 2000.

[12] M. K. Hornstein, "Design of a 460 GHz second harmonic gyrotron oscillator for use in dynamic nuclear polarization," Master's thesis, Massachusetts Institute of Technology, Department of Electrical Engineering and Computer Science, Sept. 2001.

[13] M. K. Hornstein, V. Bajaj, R. G. Griffin, K. E. Kreischer, I. Mastovsky, M. A. Shapiro, and R. J. Temkin, "Design of a 460 GHz second harmonic gyrotron oscillator for use in dynamic nuclear polarization," in *Proc. 27th Int. Conf. Infrared Millim. Waves*, R. J. Temkin, Ed., no. IEEE Cat. No. 02EX561, San Diego, CA, Sept. 2002, pp. 193–4.

[14] W. Herrmannsfeldt, "EGUN: An electron optics and gun design program," Stanford Linear Accelerator Center, Stanford, California, Technical Report SLAC-0331 UC-28, Oct. 1988.

[15] A. W. Fliflet and M. E. Read, "Use of weakly irregular waveguide theory to calculate eigenfrequencies, Q values, and RF field functions for gyrotron oscillators," *Int. J. Electron.*, vol. 51, no. 4, pp. 475–484, Oct. 1981.

[16] B. Danly and R.J.Temkin, "Generalized nonlinear harmonic gyrotron theory," *Phys. Fluids*, vol. 29, no. 2, pp. 561–567, Feb. 1986.

[17] K. Kreischer, , and R. Temkin, "Mode excitation in a gyrotron operating at the fundamental," *Int. J. Infrared Millim. Waves*, vol. 2, no. 2, pp. 175–196, Mar. 1981.

[18] I. Zarnitsina and G. Nusinovich, "Stability of single-mode self-excited oscillations in a gyromonotron," *Radiophys. Quantum Electron.*, vol. 17, no. 12, pp. 1418–1424, Dec. 1974.

[19] T. Idehara, T. Tatsukawa, I. Ogawa, T. Mori, H. Tanabe, S. Wada, G. Brand, and M. Brennan, "Competition between fundamental and second-harmonic operations in a submillimeter wave gyrotron," *Appl. Phys. Lett.*, vol. 58, no. 15, pp. 1594–1596, Apr. 1991.
[20] T. Idehara and Y. Shimizu, "Mode cooperation in a submillimeter wave gyrotron," *Phys. Plasmas*, vol. 1, no. 10, pp. 3145–3147, Oct. 1994.
[21] M. Yeddulla, G. Nusinovich, and T. Antonsen, "Start currents in an overmoded gyrotron," *Phys. Plasma*, vol. 10, no. 11, pp. 4513–4520, Nov. 2003.
[22] M. Botton, T. Antonsen, B. Levush, K. Nguyen, and A. Vlasov, "MAGY: A time-dependent code for simulation of slow and fast microwave sources," *IEEE Trans. Plasma Sci.*, vol. 26, no. 3, pp. 882–892, June 1998.
[23] K. Kreischer, T. Kimura, B. Danly, and R. Temkin, "High-power operation of a 170 GHz megawatt gyrotron," *Phys. Plasmas*, vol. 4, no. 5, pp. 1907–1914, May 1997.
[24] J. Zhao, G. Nusinovich, H. Guo, J. Rodgers, and V. Granatstein, "Axial mode locking in a harmonic-multiplying, inverted gyrotwystron," *IEEE Trans. Plasma Sci.*, vol. 28, no. 3, pp. 597–605, June 2000.

Melissa K. Hornstein (S'97) received the B.S. degree in electrical and computer engineering from Rutgers University, New Brunswick, NJ, and the M.S. degree in electrical engineering and computer science from the Massachusetts Institute of Technology (MIT), Cambridge, MA, in 1999 and 2001, respectively. She is working towards the Ph.D. degree in the Department of Electrical Engineering and Computer Science, MIT.

Since 2000, she has been a Research Assistant at the MIT Plasma Science and Fusion Center. She is involved in the design, development, testing, and analysis of a novel submillimeter wave second harmonic gyrotron oscillator as well as other projects in the millimeter and submillimeter regime. Her research interests include terahertz sources and their applications, such as enhanced nuclear magnetic resonance spectroscopy via dynamic nuclear polarization.

Vikram S. Bajaj received the B.A. degree in biochemistry and the M.S. degree in chemistry concurrently from the University of Pennsylvania (U. Penn.), Philadelphia, PA, in 2000. He is a doctoral student at the Massachusetts Institute of Technology in the Department of Chemistry (Physical Chemistry Division).

Since 2000, he has been a Research Fellow at the MIT Francis Bitter Magnet Laboratory, where his work involves structure determination of biomolecules through solid state nuclear magnetic resonance (NMR) and the development of dynamic nuclear polarization (DNP) for sensitivity enhancement in NMR spectroscopy.

Robert G. Griffin received the B.S. degree in chemistry (1964) from the University of Arkansas and the Ph.D. degree in physical chemistry (1969) from Washington University-St. Louis. He did his postdoctoral research in physical chemistry at the Massachusetts Institute of Technology (MIT) with Professor John S. Waugh.

In 1972, after completing his postdoctoral training, he assumed a staff position at the MIT Francis Bitter National Magnet Laboratory. In 1984 he was promoted to senior research scientist, and was appointed to the faculty in the Department of Chemistry, MIT in 1989. In 1992, he became director of the Francis Bitter Magnet Laboratory (FBML) and is concurrently director of the MIT-Harvard Center for Magnetic Resonance, where he had been associate director since 1989.

Professor Griffin has published more than 300 articles concerned with magnetic resonance methodology and applications of magnetic resonance (NMR and EPR) to studies of the structure and function of a variety of chemical, physical and biological systems. In the last decade this research has focused on the development of methods to perform structural studies of membrane and amyloid proteins and on the utilization of high frequency ($>$100 GHz) microwaves in EPR experiments and in the development of dynamic nuclear polarization (DNP)/NMR experiments at these frequencies. He has served numerous advisory and review panels for the National Science Foundation and the National Institutes of Health.

Kenneth E. Kreischer (M'88) received the B.S. degree in physics and the Ph.D. degree in nuclear engineering from the Massachusetts Institute of Technology (MIT), Cambridge, in 1976 and 1981, respectively.

He remained at MIT as a Principal Research Scientist with the Waves and Beams Division, MIT Plasma Science and Fusion Center. His responsibilities included the design and testing of gyrotron oscillators suitable for plasma heating applications, such as successful prototypes that produced 1–2 MW of microwave power between 100–300 GHz. Other areas of research included high-gradient accelerators operating at 17 GHz, and an RF photocathode gun capable of producing a high brightness electron beam. He was also responsible for the development of submillimeter instrumentation that has been used to improve the sensitivity of electron paramagnetic resonance (EPR) and NMR spectrometers. In 2000, he became Director of the Vacuum Electronics Technology Group, Northrop Grumman Corporation, Rolling Meadows, IL. This group is developing high-power amplifiers suitable for electronic countermeasures, communications, and radar.

Dr. Kreischer is a Member of the American Physical Society.

Ivan Mastovsky has been a research specialist at the Massachusetts Institute of Technology for over 25 years. His research interests include free electron lasers, relativistic magnetrons, high power microwave tubes, and accelerators.

Michael A. Shapiro (M'01) received the Ph.D. degree in radio physics from the University of Gorky, Gorky, Russia, in 1990.

In 1995, he joined the Plasma Science and Fusion Center, Massachusetts Institute of Technology (MIT), Cambridge, where he is currently Head of the Gyrotron Research Group. His research interests include vacuum microwave electron devices, high power gyrotrons, dynamic nuclear polarization spectroscopy, high gradient linear accelerator structures, quasi-optical millimeter-wave components, and photonic bandgap structures.

Jagadishwar R. Sirigiri (S'98, M'02) received the B.Tech. degree in Electronics and Communication Engineering from the Institute of Technology, Banaras Hindu University in 1996, and the M.S. and Ph.D degrees in Electrical Engineering and Computer Science from the Massachusetts Institute of Technology (MIT), Cambridge, MA, in 1999 and 2002, respectively.

From 1994 to 1996, he was associated with the Center of Research in Microwave Tubes, Banaras Hindu University, where his research areas included TWTs and gyro-TWTs. From 1996 to 1998, he was with Global R&D, Wipro Infotech. Ltd., where he worked in the multimedia research group. Since 2002, he has been a Posdoctoral Research Assosciate at the Plasma Science and Fusion Center at MIT. He is involved in the design and development of novel high power gyrotrons and gyrotron amplifiers at millimeter wave frequencies. His research interests include novel microwave sources and amplifiers in the millimeter and sub-millimeter regime such as the gyrotron, quasioptical structures and photonic band gap (PBG) structures and their applications in microwave vacuum electronics.

Richard J. Temkin (M'87, F'94) received the B.A. degree in physics from Harvard College, Cambridge, and the Ph.D. degree in physics from the Massachusetts Institute of Technology (MIT), Cambridge. From 1971 to 1974, he was a Postdoctoral Research Fellow in the Division of Engineering and Applied Physics, Harvard University.

Since 1974, he has been with MIT, first at the Francis Bitter National Magnet Laboratory and later at the Plasma Science and Fusion Center (PSFC) and the Department of Physics. He currently serves as a Senior Scientist in the Physics Department, as Associate Director of the PSFC, and Head of the Waves and Beams Division, PSFC. His research interests include novel vacuum electron devices such as the gyrotron and free electron laser; advanced, high-gradient electron accelerators; quasi-optical waveguides and antennas at millimeter wavelengths; plasma heating; and electron spin resonance spectroscopy. He has been the author or coauthor of over 200 published journal articles and book chapters and has been the editor of six books and conference proceedings.

Dr. Temkin is a Fellow of the IEEE, the American Physical Society and The Institute of Physics (London). He has been the recipient of the Kenneth J. Button Prize and Medal of The Institute of Physics, London and the Robert L. Woods Award of the Department of Defense for Excellence in Vacuum Electronics research.